Macromolecules

pubs.acs.org/Macromolecules
Article

Chain Dynamics of Halogenated Precision Polyethylenes in Different Crystal Polymorphs

Afiq Anuar,* Mareen Schaller, Rufina G. Alamo, and Kay Saalwächter*

Cite This: *Macromolecules* 2025, 58, 3849−3859

ABSTRACT: We investigate the crystallinity and chain dynamics of two crystalline forms I and II of bromine-substituted polyethylene, where bromine is substituted on every 21st backbone carbon −[$(CH_2)_{20}$−CHBr]−. Form I exhibits an all-*trans* planar conformation, while form II adopts a zigzag, nonplanar, herringbone-like structure with gauche conformations around the CHBr group. Static ^{1}H NMR revealed that form II has a slightly higher crystallinity compared to form I, illustrating minor crystallinity differences despite their distinct crystal structures. Both forms, however, achieve much lower crystallinity relative to typical polyethylene (PE), highlighting the pronounced effect of low Br substitution. This chain alteration also impedes chain diffusion on the time scale relevant for lamellar growth, a phenomenon commonly observed in semicrystalline PE. ^{13}C−^{1}H dipolar MAS NMR experiments indicate that form II's gauche conformers stiffen adjacent CH_2 chains, leading to lower motion amplitude in the crystalline chain stem compared to form I, which displays more uniform vibrational motion amplitude. Additionally, ^{13}C T_1-relaxation measurements reveal atypically short and distributed crystal-related T_1 values in both forms. By using ^{1}H crystal-phase filtering and spin diffusion into the near-surface crystalline stems, we detect the CH_2 in the semicrystalline interphase to be biased toward short T_1, highlighting faster local mobility down to the ns time scale close to the fold surface as compared to the core.

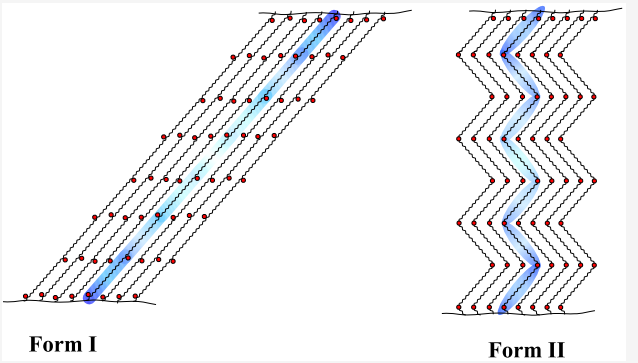

1. INTRODUCTION

Polyethylene (PE) is one of the most widely produced and extensively studied polymers due to its remarkable versatility and broad range of applications across various industries. Its unique properties, including mechanical strength, chemical resistance, and thermal stability, make it an ideal material for use ranging from packaging to automotive components. A notable feature of PE is its ability to undergo significant property modifications through the incorporation of small amounts of comonomers. These modifications can lead to substantial changes in crystallinity, chain dynamics, and mechanical performance, thereby offering opportunities to tailor materials for specific applications.[1−10] Moreover, the sparse incorporation of functional groups offers great perspectives for improved circularity of this important polymer.[10−12] For tailored and optimized mechanical properties, an in-depth understanding of the effect of such defects on the semicrystalline morphology and dynamics is obviously required.

Among the various strategies to alter PE properties, the incorporation of halogen atoms, such as bromine or chlorine, along the polymer backbone has been the focus of a number of fundamental works. Studies have shown that even small amounts of halogen (Br or Cl), whether randomly or precisely distributed along the chain backbone, play a significant role in modifying PE properties.[1,2,13] For instance, Cl-substituted polyethylenes, with Cl atoms placed at every 9th to 21st carbon, exhibit notable differences in crystallinity, melting temperatures, and crystalline structure.[4,7,9] Precision Cl substitution, synthesized via olefin metathesis polycondensation, leads to a homopolymer-like crystallization pattern, with relatively large crystal thicknesses and sharp thermal transitions.[1] In contrast, random chlorine substitution results in a nonuniform distribution of Cl atoms, broad thermal transitions, lower crystallinity, and curved, segmented lamellae.[4]

In the studied case, we are concerned with the substitution of Br at regular intervals, such as every 21st carbon atom, which induces two distinct polymorphs, as form I and form II.[7,14,15] Form I is characterized by an all-*trans* planar conformation of the polymer chains, while form II features a

Received: February 7, 2025
Revised: March 28, 2025
Accepted: April 4, 2025
Published: April 14, 2025

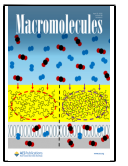

https://doi.org/10.1021/acs.macromol.5c00349
Macromolecules 2025, 58, 3849−3859

nonplanar, herringbone-like structure resulting from the formation of gauche conformers adjacent to the CHBr groups.[6,14,15] The transition between these two forms is highly sensitive to crystallization conditions, especially temperature and cooling rates.[7,14] Form I tends to form under rapid quenching conditions, while slower cooling processes favor the formation of form II.[14] Notably, form I exhibits a lower melting point compared to form II,[14] with methylene units forming layered structures and Br situated at the layer boundaries.[6] These findings underscore the potential for precise kinetic control of crystallization in novel polyolefins with tuned physical properties, facilitating the development of materials with nanostructures at the lamellar and sublamellar levels, which are not feasible in classical polyethylenes.

Despite extensive research on these two polymorphs, a detailed understanding of their crystallization and chain dynamics remains limited. Our study addresses this gap by examining the crystallinity and chain dynamics of bromine-substituted polyethylene, specifically with bromine at every 21st carbon (PE21Br), as these factors play a crucial role in crystal lamellar structure and the overall semicrystalline morphology of polymers.[16,17] Using advanced NMR techniques,[18−21] we uncover differences in crystallinity and local chain dynamics between two distinct forms of PE21Br, formed under different cooling rates. Our findings reveal that gauche-containing form II exhibits slightly higher crystallinity compared to form I, highlighting the role of kink-enabled gauche conformers in enhancing crystal packing. We also confirmed the precise Br incorporation to prevent intracrystalline chain diffusion between crystalline and amorphous chains on the same time scale of lamellar growth (or faster), a phenomenon typically observed in PE and other polymers (e.g., PEO) and a decisive factor controlling the morphology.[16,17] Furthermore, we found that both forms exhibit distinct distributions of vibrational motion amplitudes across their crystalline chain stems, with form II displaying a more complex dynamic profile due to its gauche conformers. Our ^{13}C T_1-relaxation measurements further reveal the presence of unusually pronounced fast (sub-μs) local mobility within the crystalline regions of both forms, a phenomenon not typically observed in semicrystalline polymers, but in line with the collective local motion reported in similar polymer structures with precise substitutions.[22] The shorter ^{13}C T_1-relaxation toward the fold surface suggests that these chain segments exhibit faster local mobility compared to those in the lamellar core.

This research not only enhances the understanding of the semicrystalline nature and mechanical properties of bromine-substituted polyethylenes but also demonstrates how precise chemical modifications can drastically alter polymer behavior, particularly in terms of crystal packing, molecular motion, and defect formation. Our findings contribute valuable insights for designing advanced materials with tailored mechanical characteristics, opening new avenues for the development of potentially more sustainable PE-like materials.[12]

2. EXPERIMENTAL SECTION

2.1. Materials. The PE21Br sample, a polyethylene with a bromine atom placed on every 21st backbone carbon, was synthesized via acyclic diene metathesis polymerization.[2] The characterization of its chain structure can be found in prior works.[6,14] It was reported that both forms consist of approximately 5−9 repeating units (of 21 carbon atoms length comprising the effectively large "monomer") in lamellar crystallites,[1,4,13] with small-angle X-ray scattering (SAXS) measurements showing a core crystal thickness of ∼120 ± 10 Å with a long spacing of ∼230 ± 10 Å.[7] Previous GPC measurements[6] indicated that the sample has a molecular weight (M_w) of 94 100 g/mol, with polydispersity index (PDI) of 2.2, and a Br content of 4.76 mol %. DSC experiments revealed that upon cooling from the melt at 10 °C/min, PE21Br displays a crystallization temperature (T_c) of 53 °C, and a melting temperature (T_m) of 70 °C on second heating. The dimorphism in the PE21Br crystal structure was controlled by thermal treatment. Unoriented form I was produced by rapid quenching from the melt at 75 °C to room temperature, while form II was produced by slow cooling at approximately 1 K/min. The correct polymorphic forms were confirmed by DSC experiments on the studied samples, with the expected result of their different melting points of 62 °C for form I and 71 °C for form II, see the Supporting Information (SI), Figure S1. To avoid a possible phase transition from form I to form II at high temperatures, measurements of form I were restricted to temperatures below 65 °C. SAXS data showed that the crystal lamellar thicknesses of both form I and form II were approximately the same.[7]

2.2. Crystallinity from ^{1}H NMR FIDs. ^{1}H time-domain NMR experiments were conducted on a 200 MHz Bruker Avance III spectrometer, using a static probe head with a short dead time of 2 μs. The temperature was controlled during the experiment by heated or cooled air flow, operated using a BVT300 unit with an accuracy of ±1 K and a gradient up to 0.5 K over the sample. Stepwise heating was applied to realize Figure 1, with an additional 10 min of equilibration

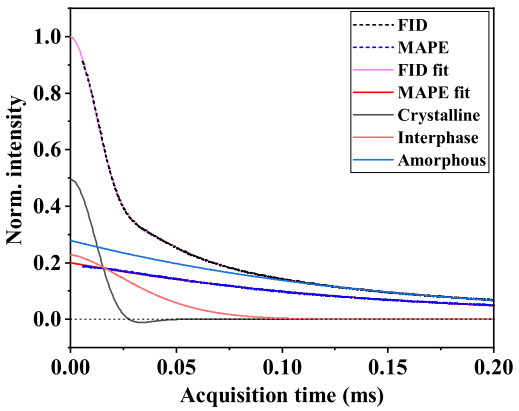

Figure 1. Decomposition of the ^{1}H NMR FID signal of PE21Br form I measured at 42 °C.

time before each NMR-FID measurement. The 90° pulse length was set to about 2 μs (corresponding to a power of 70−80 W). The recycle delay was set between 4 and 10 s, approximately 5 times the ^{1}H T_1-relaxation time of the crystalline domain, to ensure complete relaxation of the sample. The crystallinity of the samples at each temperature was determined based on the strong ^{1}H−^{1}H dipole−dipole couplings in the crystalline phase and their averaging by fast segmental dynamics in the amorphous phase. In this way, the FIDs feature 3 distinguishable T_2 components featuring fast, intermediate, and slow dipolar dephasing, associated with the crystal, interface, and amorphous fractions, respectively. The fitting equation based on this concept reads[19]

$$I_{FID}(t) = A_c \cdot e^{-(a^2t^2/2)} \cdot \frac{\sin(b \cdot t)}{b \cdot t} + A_i \cdot e^{-(t/T_{2,i}^*)^{\upsilon_i}} + A_a \cdot e^{-(t/T_{2,a}^*)^{\upsilon_a}} \quad (1)$$

where t is the acquisition time, $A_{c,i,a}$ are the amplitudes of the corresponding decaying components, $T_{2,i,a}^*$, and $\upsilon_{a,i}$ are the shape parameters (apparent T_2 and stretching exponents υ of the more mobile components), while a and b are the shape parameters of the crystalline part, where the so-called Abragamian function works well for polymers with only CH_2 groups along the main chain. From parameters a and b, the second moment of the proton line width in

https://doi.org/10.1021/acs.macromol.5c00349
Macromolecules 2025, 58, 3849−3859

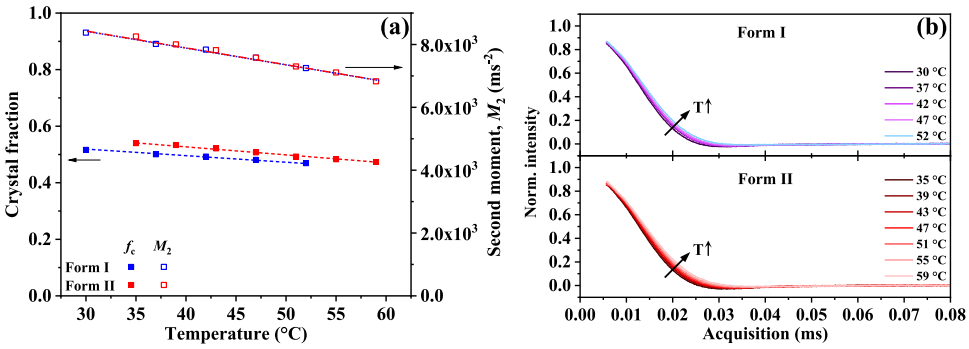

Figure 2. (a) Crystalline fraction (left scale) and the second moment M_2^H (right scale) as a function of temperature for both forms of PE21Br from ^{1}H FID measurements. (b) Normalized crystalline components of ^{1}H FID signals with temperature variations after subtraction of fitted amorphous and interface components.

the crystal can be obtained as $M_2^H = a^2 + b^2/3$. It reflects the proton density and possibly a small extent of averaging by fast local motions. Moreover, the magic and polarization echo (MAPE) pulse sequence was applied with a filter duration ranging from 0.4 to 0.7 ms to selectively attenuate the crystalline signals, facilitating component fitting and decomposition analysis.[18,19] Figure 1 shows a representative example of MAPE and FID curve fitting for PE21Br of form I measured at 42 °C. The mass crystallinity was calculated according to

$$f_c = \frac{A_c}{A_c + A_i + A_a} \tag{2}$$

2.3. ^{13}C MAS NMR Spectroscopy. All ^{13}C magic-angle spinning (MAS) measurements were conducted on a 400 MHz Bruker Avance III spectrometer with a ^{13}C Larmor frequency of 100.6 MHz using double and triple resonance magic-angle spinning (MAS) probes at a spinning frequency of 10,000 ± 3 Hz. The $\pi/2$-pulses power used was set to 40 W for ^{1}H and 140 W for ^{13}C, with corresponding pulse lengths of approximately 3 μs. ^{13}C cross-polarization (CP) spectra, which are the results of polarization from ^{1}H to ^{13}C, were employed to enhance the weak ^{13}C intensity. Due to the reduced efficiency of ^{1}H−^{13}C polarization transfer for mobile chains, a short contact time (CT) of 0.01 ms was used to suppress the contribution from amorphous domains in the spectra. ^{13}C direct polarization (DP) spectra with a short recycle delay (RD) were used to selectively detect mobile groups within the sample, setting RD to 1 s, ensuring that only signals with ^{13}C T_1-relaxation shorter than 1 s, corresponding to mobile chains, were detected.

2.4. ^{13}C T_1-Relaxation and Diffusive Exchange. The ^{13}C T_1-relaxation times provide crucial insights into the molecular dynamics of the chain segments. In this work, the ^{13}C T_1-relaxation measurements were performed using Torchia's z-filter pulse sequence applied to the ^{13}C channel after CP.[20] This method ensures that the signal decay, represented by I_τ, reaches a well-defined zero intensity. The observed signal decay can reflect either exponential T_1-relaxation or a diffusive process. The latter arises when chain motion transfers magnetization from crystalline regions to the amorphous phase, where T_1-relaxation is almost instantaneous.[23] A key signature of such diffusive behavior is a linear decay when the data are plotted as a function of the square root of time, $\sqrt{\tau}$. To distinguish between diffusive and exponential relaxation, the decay function $(1 - I_\tau/I_0)$ can be analyzed on a double-logarithmic scale against τ.[24] In this representation, a power-law decay with an exponent of 1/2 serves as an indicator of diffusive behavior, while the linear τ-dependence corresponds to exponential relaxation in the short-time limit. This approach provides an effective method of identifying and quantifying contributions of chain diffusion and T_1-relaxation.

2.5. Motional Amplitudes from ^{13}C−^{1}H DIPSHIFT NMR. The ^{13}C-detected dipolar chemical-shift correlation (DIPSHIFT) experiment,[21] which is applicable under high-resolution MAS condition, was utilized to measure the strength of the static ^{13}C−^{1}H heteronuclear dipole−dipole couplings (D_0) and motionly reduced residual coupling constant (D_{res}), provided that the rate of motion exceeds the static-limit coupling constant $D_{CH} \approx 2\pi \times 21-22$ kHz for a CH_2, which, in the case of uniaxially symmetric dynamics is commonly described by a dynamic order parameter $S = D_{res}/D_0$ that describes motion amplitudes.[25] The potentially reduced D_{res} reflects the amplitude of fast orientation fluctuations of the CH bonds in the CH_2 group with correlation times significantly below the inverse D_0, i.e., 10 μs or lower.[26] Unlike the ^{1}H−^{1}H homodipolar coupling case, the influence of interchain couplings to remote protons is much weaker; the experiment thus provides rather local information. DIPSHIFT modulation curves, with the modulation time t_1 varying between 0 and the rotor period T_{rot} were acquired for the crystalline CH_2 resonance positions using the pulse sequences described in previous works[27,28] using an initial CP and Lee−Goldburg homodecoupling. In this work, to extract the D_{res} of the CH_2 group, the intensity modulation of the CH_2 group was fitted using an analytical solution for CH_2 groups.[29]

2.6. Correlation between ^{13}C T_1-Relaxation and Order Parameter S. The T_1-relaxation times provide crucial insights into the molecular dynamics of CH_2 units in crystalline domains and are closely linked to the dynamic order parameter S derived from DIPSHIFT experiments.[30,31] The relationship between T_1-relaxation and S can be understood through spectral density function $J(\omega)$, which describes the frequency dependence of molecular motion. For motion amplitude characterized by S and a correlation time τ_c, the spectral density is expressed as

$$J(\omega) = (1 - S^2)\frac{\tau_c}{1 + (\omega\tau_c)^2} \tag{3}$$

where ω is the Larmor frequency and τ_c represents the time scale of molecular motion. The T_1-relaxation is inversely proportional to the relaxation rate, which depends on contributions from the spectral density function at different frequencies. For a heteronuclear dipolar-coupled system featuring a single motional process, T_1 can be written as

$$T_1 = \frac{1}{M_2^{CH}[J(\omega_C - \omega_H) + 3J(\omega_C) + 6J(\omega_C + \omega_H)]} \tag{4}$$

where M_2^{CH} is the dipolar coupling second moment, and ω_C and ω_H are the Larmor frequencies of ^{13}C and ^{1}H, respectively. The terms $J(\omega_C - \omega_H)$, $J(\omega_C)$, and $J(\omega_C + \omega_H)$ represent spectral densities at specific frequencies, corresponding to the dipolar interactions. The $M_2^{CH_2}$ for CH_2 group can be calculated as

$$M_2^{CH_2} = \frac{1}{5}\frac{\gamma_C^2\gamma_H^2\hbar^2}{r^6} \tag{5}$$

where γ_C^2 and γ_H are the gyromagnetic ratios of ^{13}C and ^{1}H, $\hbar$ is the reduced Plank constant, and r is the C−H internuclear distance. For r = 1.08 Å, $M_2^{CH_2}$ evaluates to 4.2×10^{10} s^{-2}.

Higher S-values, corresponding to more restricted molecular motion, result in longer T_1-relaxation times, while lower S-values,

https://doi.org/10.1021/acs.macromol.5c00349
Macromolecules 2025, 58, 3849−3859

indicative of greater motion amplitudes, yield shorter T_1 values. The given relationships enable the estimation of T_1-relaxation times based on S-values obtained from the DIPSHIFT experiment. In this study, the experimentally measured T_1 values were compared with theoretical approximations derived from the single-motion spectral density function and the corresponding S-values.

2.7. ^{13}C T_1 after ^1H Spin Diffusion. The Goldman-Shen (GS) dipolar filter experiment[32] was performed to investigate crystal surface segments by using $T_{2,H}$ filtering to suppress the strongly dipolar-coupled crystalline signal, and ^1H spin diffusion to transfer ^1H magnetizations from amorphous domain into crystalline surface, followed by cross-polarization to ^{13}C. During the $T_{2,H}$ filter, which had a duration around 0.4 ms, the $^{13}C-^1H$ dipolar interaction was decoupled by irradiation on the ^{13}C channel. The ^1H spin diffusion time (after the $T_{2,H}$ filter, and before cross-polarization) ranged up from 1 ms to 1 s. Afterward, cross-polarization from ^1H to ^{13}C was performed to observe the ^{13}C signal and to study its T_1 relaxation decay using Torchia's pulse sequence. To avoid too-strong averaging of the $^1H-^1H$ dipolar couplings, these experiments were conducted at a moderate MAS rate of 5 kHz.

3. RESULTS AND DISCUSSION

3.1. Crystallinity. The crystallinity of both forms of PE21Br was investigated by using ^1H FID measurements. Figure 2(a) shows the crystallinity and the related dipolar second moment (M_2) of both forms as a function of temperature. Both forms exhibit crystallinity below 55%, which is significantly lower than typical semicrystalline PE (usually 70−80%),[33,34] highlighting the substantial impact of the precision inclusion of Br atoms on PE crystal formation. Previously, Zhang et al.[7] found by SAXS that both forms have core crystal thicknesses of ∼120 ± 10 Å with long spacings of ∼230 ± 10 Å, resulting in "linear" crystallinities of around ∼52%, consistent with our ^1H FID measurements. When comparing the two forms, form II shows slightly higher crystallinity than form I. While systematic errors related to the fitting are estimated to about ∼5%, we consider the 2−3% differences significant. In previous work,[7] a higher DSC melting peak in crystallized samples of form II compared to form I implies a more stable phase, and suggested that form II may have thicker crystallites than form I. Nevertheless, both forms have comparable M_2^H, indicating similar packing environments.[7,15]

The gradual decrease in M_2 with increasing temperature reflects lattice expansion, typically indicating the absence of fast intracrystalline chain dynamics (ICD) up to 0.2 ms.[34,35] Compared to semicrystalline PE (M_2^H = 12,600−13,000 ms^{-2}), the M_2^H of PE21Br is significantly lower, as shown in the SI, Figure S2.[34] This reduction is due to the structural impact of Br substitution. Although Br is only present at every 21st carbon, its bulkiness increases the unit cell dimensions and $^1H-^1H$ distances, weakening dipolar couplings and reducing local proton density.[1,6] These factors contribute to the significantly lower M_2 value in PE21Br. The much lower M_2 in PE21Br compared to PE also suggests that the chain packing in PE is much more efficient than in PE21Br, explaining the lower melting temperature of PE21Br.[4,7] Figure 2(b) shows normalized ^1H FID crystalline lineshapes with temperature, probing for ICD typically observed in semicrystalline PE.[16,17,23,34,36] The minimal changes in lineshapes also suggest no fast ICD, only small-angle vibration and thermal expansion.[34,35] Given the low crystallinity and temperature sensitivity shown in Figure 2(a), it is further suggested that neither form exhibits ICD on fast time scales.[16,17,24] To further investigate chain dynamics at slower time scales and local vibration motion in both forms, we conducted several ^{13}C MAS NMR experiments.

3.2. Assignment and Analysis of ^{13}C MAS Spectra in PE21Br Polymorphs. Prior to investigating chain dynamics, it is essential to assign ^{13}C resonances. Figure 3 compares the ^{13}C CP MAS spectra between the two polymorphic forms of PE21Br. The ^{13}C assignments are based on previous studies,[1,4,15] where the CH_2 group adjacent to CHBr is labeled as α-CH_2 and the subsequent CH_2 group is labeled as β-CH_2. These assignments are further confirmed by CP contact time variations and comparisons of CP and DP spectra shown in the SI, Figures S3 and S4, respectively. The crystal and amorphous peaks of each ^{13}C site are distinguished by the γ-gauche effect.[37] The amorphous peaks of both forms remain constant, while differences in the crystal peaks of α-CH_2 (α-$CH_{2,c}$) and CH (CH_c) highlight the dissimilarity in the crystalline chain structures between the two forms. The differences in the α-$CH_{2,c}$ and CH_c between the forms are attributed to the presence of gauche conformations adjacent to the Br atom in form II, whereas form I exhibits an all-*trans* conformation.[6,15] The shifts of the crystalline inner-CH_2 (inner-$CH_{2,c}$) peaks are identical in both forms, indicating that the inner-$CH_{2,c}$ in both forms maintain the same all-*trans* conformation.[6,15] The consistency of the amorphous peaks further supports the previous differentiation between crystalline and amorphous peaks.[6,15] With the ^{13}C peaks now identified, an investigation into the crystalline chain dynamics of both forms can proceed.

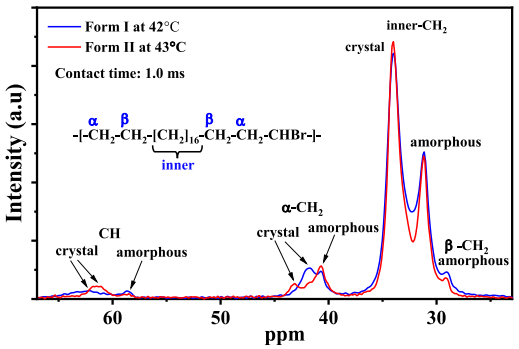

Figure 3. ^{13}C CP MAS spectra with a 1.0 ms contact time for PE21Br form I and form II.

3.3. Vibrational Motion Amplitude in PE21Br Crystals. The DIPSHIFT experiment[21] was utilized to assess the submicrosecond time scale local vibrational amplitudes of the $CH_{2,c}$ groups in PE21Br crystal chains by measuring the motionly reduced residual dipolar coupling constant, D_{res}. An analytical solution, detailed in Hackel et al.[29] was used for the fits as shown in the SI (Figure S5) to extract the D_{res} values for both forms. A lower D_{res} value indicates a greater vibrational motion amplitude. To facilitate interpretation, the D_{res} values were normalized against the rigid-limit dipolar coupling constant, D_0 measured for the CH_2 group of crystalline glycin under the same conditions, as shown in Figure S6(a), yielding the dynamic order parameter, S. Figure 4 shows the S values of (a) inner-$CH_{2,c}$ and (b) α-$CH_{2,c}$ of both forms, with the results compared to the previously published data on HDPE from Bärenwald et al.,[38] see also Figure S6(b).

The results indicate that inner-$CH_{2,c}$ in form II exhibits higher S values compared to that in form I across all temperatures, suggesting less vibrational motion in inner-

https://doi.org/10.1021/acs.macromol.5c00349
Macromolecules 2025, 58, 3849−3859

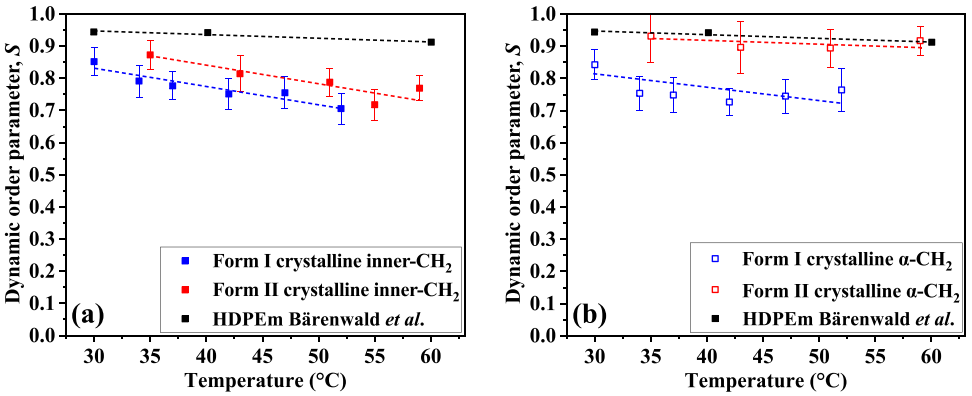

Figure 4. Dynamic order parameters of (a) crystalline inner-CH_2 (inner-$CH_{2,c}$) and (b) crystalline α-CH_2 (α-$CH_{2,c}$) in both PE21Br forms, extracted from $^{13}C-^{1}H$ dipolar coupling measurements using the DIPSHIFT experiment. HDPE is included for comparison. The dashed lines are a guide to the eye.

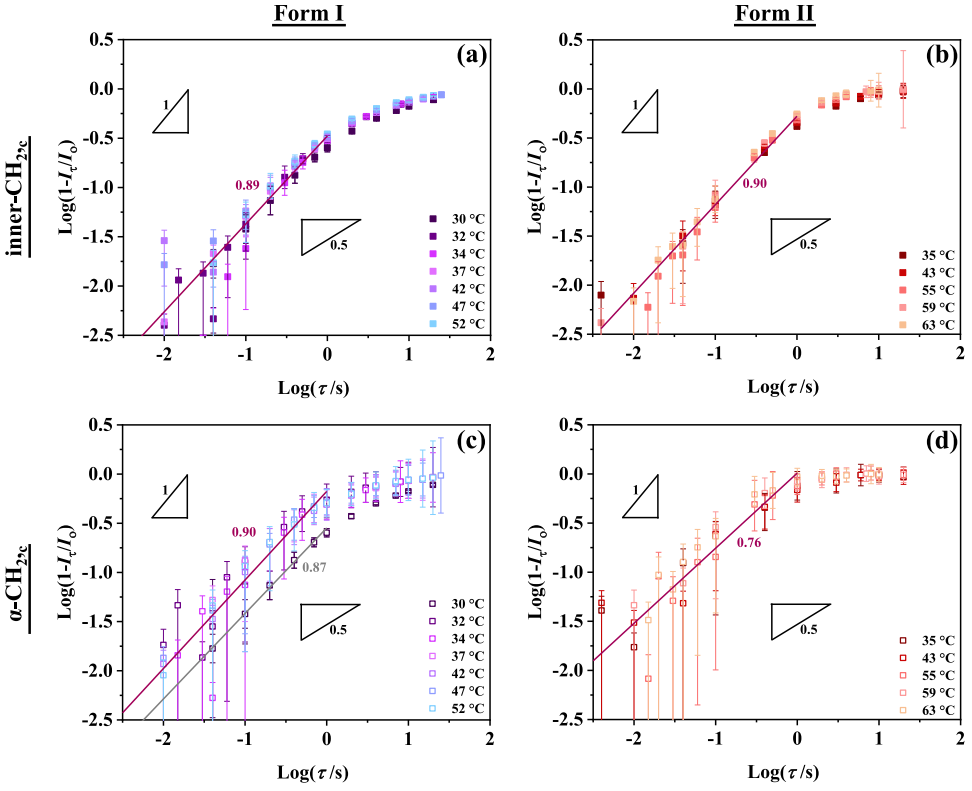

Figure 5. Plots of $\log(1 - (I_\tau/I_0))$ versus $\log(\tau)$ for inner-$CH_{2,c}$ of (a) form I and (b) form II as well as for α-$CH_{2,c}$ of (c) form I and (d) form II. The as-measured relaxation decays are shown in Figure S7.

$CH_{2,c}$ of form II than form I. We expect that the lower motion amplitude of the crystalline stem of form II contributes to its higher melting point. Both S values decrease with increasing temperature, which is typical, as thermal energy enhances local mobility.[38] In comparison, the crystalline CH_2 ($CH_{2,c}$) of HDPE exhibit higher S values than inner-$CH_{2,c}$ of both forms at all measured temperatures. This indicates that the $CH_{2,c}$ segments in HDPE have a lower vibrational motion amplitude compared with those in the PE21Br forms. This reduced vibrational motion in HDPE may be attributed to its highly packed crystalline structure,[1,6] which correlates with the significantly high M_2^H in Figure S2, resulting in more restricted vibrational freedom of the chain.

Notably, Figure 4(b) indicates that the α-$CH_{2,c}$ of form II has a higher and nearly T-independent S than its inner-$CH_{2,c}$ counterpart, actually close to the HDPE value. The lower vibrational motion amplitude of α-$CH_{2,c}$ likely results from the highly ordered gauched-adjacent Br layers in its herringbone-like crystalline structure, which created more restricted space and simultaneously leads to lower vibrational amplitude on the inner-$CH_{2,c}$ segments.[6,14,15] The relatively low vibrational amplitude observed in form II's crystalline chains also suggests better crystal packing. As for the all-*trans* crystalline structure of form I, the vibrational motion is distributed more homogeneously along the stem in the long unit cell. Although the final two data points of α-$CH_{2,c}$ appear to show a slight upturn in S, we attribute this to experimental uncertainty rather than a physically meaningful increase. This observation underscores the influence of chain conformation on the

https://doi.org/10.1021/acs.macromol.5c00349
Macromolecules 2025, 58, 3849−3859

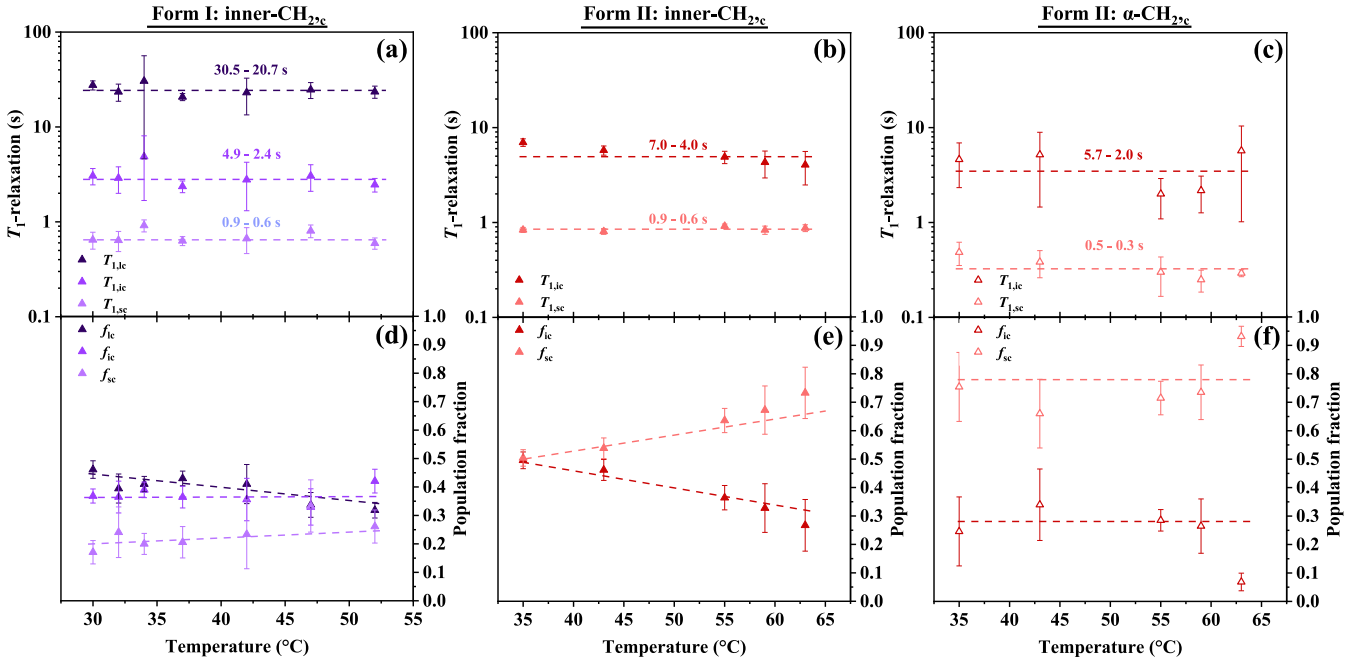

Figure 6. ^{13}C T_1-relaxation times for inner-$CH_{2,c}$ of (a) form I, (b) form II, and (c) α-$CH_{2,c}$ of form II, along with their respective ^{13}C T_1-relaxation fractions, f_{xc} (x = l,i,s), for (d) form I and (e, f) form II. For simplicity, only α-$CH_{2,c}$ analyses on form II are included, as the trends observed in form I are consistent and provided in Figure S9. These data were extracted from the multiexponential fits of the measurements shown in Figure S7(a,b,d). The $T_{1,s}$ represents ^{13}C T_1-relaxation times less than 1 s, associated with more mobile chains, while $T_{1,l}$ refers to ^{13}C T_1-relaxation times greater than 10 s, corresponding to rather rigid chains (i denoting intermediate).

distribution of local vibrational motion amplitudes along the crystallite stem.

3.4. Local Mobility and Interface Analysis in PE21Br Crystals. The presence of the ICD, which results in chain sliding diffusion between the crystalline and amorphous regions, can be detected via ^{13}C T_1-relaxation measurements. In case where chain diffusion occurs, the ^{13}C T_1 decays linearly with the square root of time in the initial phase, following a 1D free-diffusion model.[24,38−41] In contrast, in nondiffusive cases, the ^{13}C T_1 decays exponentially.[35] In our previous work,[24] we demonstrated a simple approach to distinguish between exponential and square-root decay. In the case of 1D free-diffusion, the initial decay can expressed as[24,38−41]

$$\frac{I_\tau}{I_0} = 1 - \frac{\sqrt{2D}}{d_c}\sqrt{\tau} \tag{6}$$

where $I(\tau)/I(\tau = 0)$ is the normalized decay intensity and D is the diffusion coefficient of the chain along the stem direction. For analysis purposes, this can be rewritten as

$$\log\left(1 - \frac{I_\tau}{I_0}\right) = \frac{1}{2}\log\tau + \log\frac{\sqrt{2D}}{d_c} \tag{7}$$

This forms the basis for a log−log plot, which would reveal the 1/2 power-law exponent in the initial slope in the diffusive case. Figure 5 shows $\log(1 - (I_\tau/I_0))$ versus $\log(\tau)$ plots for the inner-$CH_{2,c}$ and α-$CH_{2,c}$ of both forms, extracted from T_1-relaxation measurements (see the SI, Figure S7, for the as-measured relaxation decays). All plots feature initial slopes rather different from 0.5 and near to 1, indicating a near-exponential decay and the absence of chain diffusion in the crystallites of both forms.[24] To be sure that a potential diffusive process is not masked by the comparably (and surprisingly) short T_1 relaxation times of the crystalline carbons (to be addressed below), we have conducted ^{13}C 2D exchange NMR experiments, see Figure S8. No exchange peak between the crystal and amorphous peaks of inner-CH_2 in both forms could be detected, further confirming the absence of chain diffusion and designating these as crystal-fixed polymers. This correlates with the low crystallinity observed in Figure 2(a), a characteristic typically found in crystal-fixed polymers.[16,17,35] Since there is no detectable ICD in both forms, we now proceed with a more detailed analysis of the T_1 decay in these crystallites.

In a rigid semicrystalline system, ^{13}C nuclei within the crystalline domains typically exhibit T_1-relaxation times longer than 10 s ($T_{1,l}$), with small contributions from interface region or crystallite surface, where T_1 ranges between 1 to 10 s ($T_{1,i}$). In contrast, ^{13}C nuclei in the amorphous domains, characterized as mobile chains, have T_1 values shorter than 1 s ($T_{1,s}$). Figure 6 displays the ^{13}C T_1-relaxation times found in inner-$CH_{2,c}$ (panels a and b), along with their respective fractions (panels d and e) for both forms. Here, the subscript "c" denotes crystalline peaks; for example, $T_{1,lc}$ and f_{lc}, represent the long T_1-relaxation component and its corresponding fraction in the crystal.

Surprisingly, the $T_{1,sc}$ component associated with a dynamically modified population was also detected in inner-$CH_{2,c}$ in both forms, together with appreciable fractions of f_{ic}. The rapid magnetization decay associated with $T_{1,sc}$ can be seen from the unprocessed data in the SI, Figure S7, and is also evident in DP experiments with a 1 s recycle delay in Figure S4, which is atypical for semicrystalline polymers. Additionally, the fraction f_{sc} increases with temperature in both forms indicating that more inner-$CH_{2,c}$ units exhibit unusually high fast small-angle mobility at elevated temperatures. Notably, no $T_{1,lc}$ was detected in inner-$CH_{2,c}$ of form II, suggesting the complete absence of the expected rigid environment in this

https://doi.org/10.1021/acs.macromol.5c00349
Macromolecules 2025, 58, 3849−3859

chain region, a point that will be further discussed later. While we carefully analyzed the multiexponential fits to obtain estimates of the size of the populations and their associated T_1, we acknowledge potential overfitting on inner-$CH_{2,c}$ of form I in Figure 6(a,d). Therefore, a detailed comparison between biexponential and triexponential fits of inner-$CH_{2,c}$ is provided in the SI, Figures S10−S12. In summary, the residuals from triexponential fits are consistently lower and thus meaningful across all temperatures, demonstrating a better fit. The validity of the temperature-dependent trends in f_c populations, which are subjected to concerns regarding potential fitting artifacts, is also addressed in Figure S12. We should of course be aware that our finite-components fitting may just be a parametrization of a distribution of unknown shape.

^{13}C T_1-relaxation measurements of the α-$CH_{2,c}$ peak, presented in Figure 6(c,f), also detected short $T_{1,sc}$ in both forms. To streamline the discussion, form II is here emphasized, as the trends and behavior observed for form I are consistent with those of form II (see Figure S9 for results on form I). Notably, similar to inner-$CH_{2,c}$ of form II, no $T_{1,lc}$ population was fitted for α-$CH_{2,c}$ in either form, indicating that the α-$CH_{2,c}$ always features a distinct level of vibrational motions. When comparing the $T_{1,sc}$ values of α-$CH_{2,c}$ in Figure 6(c) with those of inner-$CH_{2,c}$ in Figure 6(a,b), α-$CH_{2,c}$ generally exhibits shorter T_1-relaxation times, suggesting faster molecular mobility in α-$CH_{2,c}$. Additionally, both forms show that the fraction f_{sc} of α-$CH_{2,c}$ remains relatively constant upon heating. The insensitivity of f_{sc} and f_{ic} to temperature for α-$CH_{2,c}$ further supports the exclusion of ICD, as f_s would typically increase with heating if ICD were present.

The apparent insensitivity of $T_{1,c}$ values to temperature in Figure 6(a−c) raises concerns about the reliability of the analyses, as T_1 is expected to exhibit a temperature dependence. Furthermore, tentatively associating shorter T_1 values with increased (faster) vibrational mobility requires that the T_1 values lie within the slow-motion branch of the dependence of T_1 on correlation time τ_c (see eq 3), i.e., heating should lead to decreasing correlation time and thus shorter T_1. This issue can be addressed by calculating the rate-averaged relaxation times $\langle T_{1,c}\rangle$, which better reflect the collective $T_{1,c}$ behavior and indeed do reveal temperature-dependent trends that are otherwise obscured by the distribution of $T_{1,c}$ populations. This is shown in the SI, see Figure S13. Additionally, the trends in $\langle T_{1,c}\rangle$ also support the observation that α-$CH_{2,c}$ generally exhibits shorter T_1-relaxation times than inner-$CH_{2,c}$ in both forms.

The absence of $T_{1,lc}$ in form II, despite its higher order parameter S compared to that in form I, initially appears inconsistent. The DIPSHIFT measurements in Figure 4 showed that form II has a higher S, and the S for α-$CH_{2,c}$ is even higher than that of inner-$CH_{2,c}$. However, their $T_{1,c}$ values in Figure 6 exhibit the opposite trend. To clarify this, possible $T_{1,c}$ ranges were estimated based on a single-motion model and the S values measured by DIPSHIFT. We stress that the lack of physical insight into setting up a specific motional model and the lack of a wider range of data (e.g., field-dependent T_1 results) necessarily restrict the discussion to the use of a single-motion model. This appears justified also in view of the rather small motional amplitudes, as reflected in the high S values.

The results shown in the SI, Figure S14, demonstrate that all the detected $T_{1,c}$ populations fall within the expected range despite rather high order parameters if only the correlation times are varied between a few hundred down to about 1 ns, confirming consistency with the measured S values. While we are not able to judge a possible gradient of order parameters, these evaluations clearly show that the detected short-$T_{1,s}$ populations indeed lie near the T_1 minima of the small-angle vibrational motions with τ_c in the 1 ns range, explaining the weak temperature dependence observed in Figure 6, which is more evident in $\langle T_{1,c}\rangle$ rather than in individual $T_{1,c}$ populations. Notably, the regions with long $T_{1,l}$ have much longer apparent τ_c into the μs range, i.e., rather slow for actual elastic vibrations. Thus, the observed small-angle motions are likely collective motions comprising a larger number of carbons. We can also envision a convection of conformational defects into the crystalline stems (ultimately being responsible for the ICD process in, e.g., PE) that would not propagate along the whole stem but return to the originating fold surface and be annihilated there.

While these insights provide a detailed picture of the complex local dynamics within the crystalline regions, the experiments capture only the behavior of the polymer chains across the whole crystal. The coexistence of crystalline chain parts with widely different T_1, associated with different vibrational correlation times, remains a peculiarity that to our knowledge has not been observed before. To obtain a more comprehensive picture of the overall chain dynamics in their semicrystalline structure, detailed investigation on the interphase region between the crystalline and amorphous regions is required, as these areas often exhibit significant dynamics, which plays a crucial role in influencing the material's overall properties. We have thus performed ^1H dipolar filter experiments so as to check the possibility that the observed dynamic inhomogeneity may arise not from the variation within the unit cell (which can be excluded on the basis of comparing inner-$CH_{2,c}$ and α-$CH_{2,c}$ showing similarly distributed T_1), but from the variation along the crystalline stem away from the fold surface.

To investigate the local chain dynamics close to the interface, the ^{13}C T_1-relaxation measurements were performed on the interface-dominated signal using the Goldman-Shen (GS) dipolar filter experiment. This experiment filters out the crystalline signal and then allows the ^1H magnetization to diffuse from the amorphous region into the near-surface crystalline region for certain amounts of time, as detailed in the SI, Figure S15. Figure 7(a) shows the ^{13}C T_1-relaxation results of near-surface-dominated spectra produced by the GS-dipolar filter at 40 °C, compared with the unfiltered ^{13}C T_1-relaxation decay at 42 °C, which correspond to the total inner-$CH_{2,c}$ in the crystalline phase. The results show that the GS-filtered T_1 on inner-$CH_{2,c}$ are strongly biased toward shorter T_1, where a short CP of 0.1 ms was used to ensure locality of the measurement and that we are probing the crystal domain as reflected by a high order parameter S. In this way, we can prove that the inner-$CH_{2,c}$ in unit cells near the interface are the ones that feature the surprisingly short T_1 values. It is worth noting that the interphase region likely exhibits a gradient in local chain mobility rather than a single uniform environment. Nonetheless, the distinctly shorter T_1 relaxation observed in our GS-filtered data confirms that, on average, the interface segments are significantly more mobile than the interior crystalline stems. This conclusion is robust despite the possibility of some local dynamic heterogeneity in fold-surface-related motions. On the side, we note that the small-angle motions retain a high level of interproton dipolar couplings

https://doi.org/10.1021/acs.macromol.5c00349
Macromolecules 2025, 58, 3849−3859

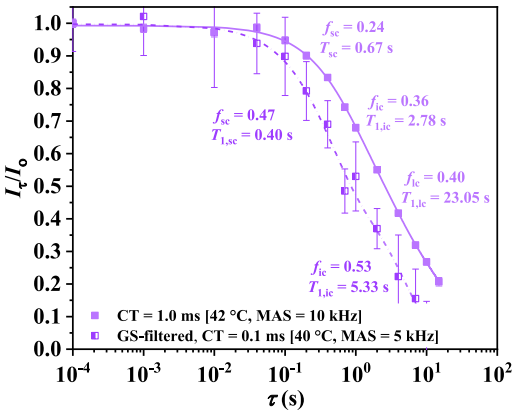

Figure 7. Goldman-Shen dipolar-filter-based ^{13}C T_1-relaxation measurement of crystalline inner-CH_2 near the fold surface of form I at 5 kHz MAS with CT = 0.1 ms and a spin diffusion delay of 10 ms. The result is compared with the significantly slower ^{13}C T_1-relaxation of the whole crystal from Figure S5(a).

and thus do not modify the spin diffusion process in any significant way.

3.5. Schematic of Local Chain Dynamics in PE21Br Polymorphs. Combining the DIPSHIFT and T_1-relaxation analyses, which are associated with local chain motion amplitudes and mobility, respectively, provides a complex picture of the overall local chain dynamics in the crystalline regions of both forms. This complexity arises from the superposition of signals from individual ^{13}C atoms within the crystal structures. Therefore, a step-by-step interpretation, from CH_2 to whole-lamella scale, shall be provided. To aid in this explanation, a simple schematic illustrating differences in local dynamics of both forms, involving both amplitudes and time scales of motion, is shown in Figure 8.

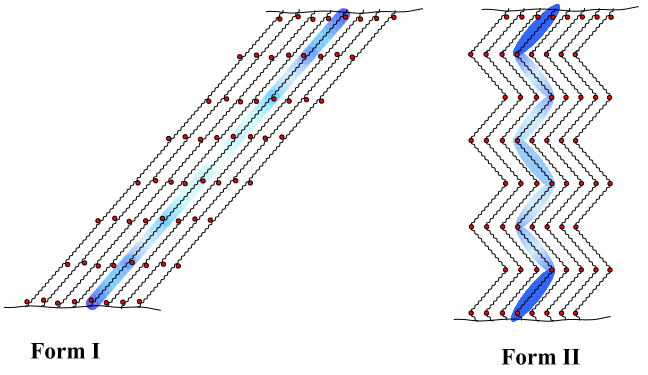

Figure 8. Schematic representation of local dynamics on the lamellar scale for (a) form I and (b) form II, with red circles corresponding to Br atoms. Dark-blue areas indicate regions of faster mobility (nanosecond scale), while white areas represent slower mobility. The wider the colored area, the greater the motion amplitude.

At the monomer scale (forming the unit cell of 21 carbons length), based on DIPSHIFT measurements in Figure 4(a,b), both forms exhibit different distributions of motion amplitudes. In form I, the motion amplitudes are distributed homogeneously along the length of the monomer, whereas in form II, they decrease near the gauche conformers (having a higher-order parameter). In Figure 8, this is illustrated by the size of colored areas: in form I, the size of colored area along the chain is uniform, while in form II, an oval-shaped colored area represents the reduced motion amplitude near the gauche conformers. Based on the temperature dependence of S, the colored areas in both forms should widen with heating, except near the gauche conformers in form II.

Moving to the T_1-relaxation analyses in Figures 6 and 7 that have been shown to be more sensitive to the time scale of motion, both forms show shorter T_1 for α-$CH_{2,c}$ compared to inner-$CH_{2,c}$. This indicates that the local dynamics of the outer carbons in a monomer, particularly near the Br atoms, generally have a faster vibrational mobility than those of the inner monomer segments. In Figure 8, this is represented by the more intense blue color near the Br atoms, indicating greater mobility compared to the more sluggish monomer center. This monomer-scale dynamic heterogeneity can be compared to the observations local and collective motion reported by Wei et al.,[22] who described twisting-like motions along a PE backbone with regularly spaced methyl groups, a structure quite similar to PE21Br. Interestingly, Wei et al.[22] observed that the motion amplitude is smaller at the monomer center and decreases as the length of the all-*trans* CH_2 segment increases, which is contrary to our case, where the amplitude is larger (order parameter is lower) in the monomer center. Thus, the chemical nature of the precisely placed "defect" plays a nontrivial role.

At the crystalline lamellar scale, the different crystalline chain structures of the two forms feature distinct local dynamics. In the all-*trans* crystalline structure of form I, the ^{13}C T_1-relaxation based on the Goldman-Shen dipolar filter in Figure 7 reveals that monomers close to the fold surface exhibit local mobility faster than that in the lamellar core. This suggests that the time scale of locally detected but likely collective motion decreases toward the crystal core, causing inner-CH_2 groups located at the core to become apparently more rigid, explaining the long detected $T_{1,lc}$ in inner-$CH_{2,c}$. In contrast, form II exhibits a qualitatively different local chain mobility profile. Its herringbone-like crystalline structure, where the monomer units are tilted in alternating directions, does not support a gradual decrease in the time scale of collective vibrations but enables faster vibrations (curiously associated with smaller angles, i.e., higher-order parameters) around the gauche conformers. In Figure 8, the reduced blue intensity toward the crystallite core in form I represents increasingly slow collective vibrations, while in form II, the α-$CH_{2,c}$ feature faster local vibrations all along the stem.

Based on the observed temperature dependencies of T_1 in Figure 6, the inner-CH_2 groups speed up more with heating as compared to the α-CH_2 groups near Br atoms. In Figure 8, this means that in both forms, the blue intensity at the monomer center should increase with heating, while the blue color near Br remains more constant. An analysis of these observations in terms of possible phonon excitations in this interesting class of materials would be highly worthwhile, but is beyond the scope of this work.

4. CONCLUSIONS

In conclusion, our study reveals subtle differences in crystal packing with distinct local chain dynamics between the two forms of PE21Br, which were formed at different cooling rates. ^1H FID measurements show that form II, containing gauche conformations, exhibits slightly higher crystallinity than form I. This finding supports a possibility of thicker crystal lamella in form II, as suggested in previous studies.[14,15] Additionally, both

https://doi.org/10.1021/acs.macromol.5c00349
Macromolecules 2025, 58, 3849−3859

forms exhibit significantly lower crystallinity compared to typical PE, emphasizing the pronounced effect of low but precise Br incorporation in hindering crystallization. The minimal changes observed in the normalized ^{1}H crystalline lineshapes with temperature suggest only very restricted movement of the crystal chain stems and an absence of fast intracrystalline chain diffusion, correlating with reduced crystallinity and pronounced decrease with temperature, which is typically observed in crystal-fixed polymers.

Measurements of dynamic order parameters S based upon ^{13}C−^{1}H dipolar couplings reveal that form I displays homogeneous vibrational motion along the chain stem, while form II shows a more uneven distribution of motion amplitudes. Specifically, the order parameter of the α-$CH_{2,c}$ groups in form II is notably lower than that of the inner-$CH_{2,c}$ groups, suggesting greater rigidity near the gauche conformers. This complex distribution of motion in the herringbone structure underscores the influence of the gauche conformers in the herringbone structure on the local dynamics and the impact on macroscopic properties, such as the melting point.

Analyses of ^{13}C T_1-relaxation decays provide valuable insight into the chain dynamics within the crystalline regions of both forms. Log−log analysis of the normalized signal decay, log $(1-I(\tau)/I(\tau = 0))$, confirms the absence of slow intracrystalline chain diffusion that could be relevant on the time scale of lamellar growth, a feature characteristic of crystal-fixed polymers, consistent with observation from ^{1}H FIDs. This highlights the substantial impact of low but precise Br substitution on hindering chain sliding between the crystal and amorphous regions, typically observed in PE.

A closer look at the crystal-related ^{13}C T_1-relaxation decays reveals a multicomponent nature with a surprisingly short T_1 population in the second range, not typically found for polyethylene-like polymer crystals. ^{13}C T_1-relaxation decays detected after a ^{1}H dipolar filter of the mobile-phase signal and a short spin diffusion delay reveal that these short-T_1 populations are preferentially located close to the fold surface of the lamellae. Model calculations of the T_1-relaxation times reveal that the short-T_1 populations can be reconciled with high local order parameters, being related to ns-time scale motions near the T_1 minimum, while its temperature dependence reveals that the related process is much slower for the longer-T_1 populations.

Taking these findings together, the overall picture of the dynamics is complex and features rather nonintuitive relations of the amplitude of motion and its time scale. In all-trans form I, the order parameter decreases with heating. The motional correlation time ranging from the μs to the ns range features a gradient toward slower motion from the fold surface into the interior of the lamellae but without large variations across the long monomer unit. In contrast, in form II the α-CH_2 groups near the gauche conformers exhibit a comparably high and T-independent order parameter and show lower T_1 and thus overall faster small-angle mobility than the long CH_2 stretches in the monomer center. Again, the correlation time shows a gradient toward the lamellar center, with even less segments featuring the long T_1 typical for pure PE crystals. These observations stand in notable contrast to an earlier study of fast motions in precision PE with methyl groups instead of bromine,[22] where the defect sites showed substantially increased rather than decreased motional amplitude.

Our findings underscore the intricate, nontrivial relationships between chemical modifications, crystalline structures, and the local as well as chain dynamics in PE-like materials, as also highlighted by earlier NMR studies of precision polyesters.[3] We expect such complex dynamics to impact the physical and mechanical properties of these materials, which is illustrated by the melting points of forms I and II, which differ by about 10 K despite the very similar morphologies (crystallinity, long spacing). Mechanical testing was so far not possible due to the currently available low quantities of these materials. In view of the growing importance of PEs with sparse comonomers enabling better recycling,[8,10−12] these complex changes deserve closer scrutiny in the future. The suite of advanced NMR methods can be straightforwardly be applied to other polymorphic polymers such as precision polyacetals[8] or long-spaced polyesters and polycarbonates.[3,11] As an outlook, first results on randomly carbonyl-modified PE[10] indicate that the intracrystalline chain diffusion is retained in this case. This will be the subject of our forthcoming work.

■ ASSOCIATED CONTENT

Data Availability Statement

The data sets generated and analyzed for this study as they appear in the figures of this article and the Supporting Information can be found in the Zenodo repository, DOI: 10.5281/zenodo.14999084.

Supporting Information

The Supporting Information is available free of charge at https://pubs.acs.org/doi/10.1021/acs.macromol.5c00349.

DSC results (Figure S1), comparison of ^{1}H second moments (Figure S2), CP contact time variation in ^{13}C spectra (Figure S3), comparison of ^{13}C CP and DP spectra (Figure S4), ^{13}C−^{1}H DIPSHIFT results and fits (Figure S5), ^{13}C−^{1}H DIPSHIFT reference data (Figure S6), ^{13}C T_1 relaxation decays (Figure S7), ^{13}C 2D exchange NMR spectra (Figure S8), ^{13}C T_1 relaxation components of α-$CH_{2,c}$ in form I (Figure S9), assessment of ^{13}C T_1 relaxation component decomposition (Figures S10−S12), temperature dependence of rate-averaged ^{13}C T_1 (Figure S13), ^{13}C T_1 predictions based upon measured order parameters (Figure S14), and dipolar-filtered ^{13}C spectra with variable spin diffusion time (Figures S15) (PDF)

■ AUTHOR INFORMATION

Corresponding Authors

Afiq Anuar − *Institut für Physik, Martin-Luther-Universität Halle-Wittenberg, 06099 Halle (Saale), Germany*; Email: mohd-afiq.bin-anuar@physik.uni-halle.de

Kay Saalwächter − *Institut für Physik, Martin-Luther-Universität Halle-Wittenberg, 06099 Halle (Saale), Germany*; orcid.org/0000-0002-6246-4770; Email: kay.saalwaechter@physik.uni-halle.de; www.physik.uni-halle.de/nmr

Authors

Mareen Schaller − *Institute for Applied Materials (IAM), Karlsruhe Institute of Technology (KIT), 76344 Eggenstein-Leopoldshafen, Germany*; orcid.org/0000-0001-6589-2087

Rufina G. Alamo − *Department of Chemical and Biomedical Engineering, FAMU-FSU College of Engineering, Tallahasee,*

Florida 32310, United States; orcid.org/0000-0002-3061-499X

Complete contact information is available at: https://pubs.acs.org/10.1021/acs.macromol.5c00349

Notes

The authors declare no competing financial interest.

■ ACKNOWLEDGMENTS

Financial support by the Deutsche Forschungsgemeinschaft (DFG) in the framework of the SFB-TRR 102 (project-ID 189853844, project A1) and the National Science Foundation (NSF) of the USA (Polymers Program, DMR 2154026) is gratefully acknowledged. We thank Alexey Krushelnitsky for his valuable advice concerning the calculation of T_1 relaxation times.

■ REFERENCES

(1) Boz, E.; Wagener, K. B.; Ghosal, A.; Fu, R.; Alamo, R. G. Synthesis and crystallization of precision admet polyolefins containing halogens. *Macromolecules* **2006**, *39*, 4437−4447.

(2) Boz, E.; Nemeth, A. J.; Alamo, R. G.; Wagener, K. B. Precision ethylene/vinyl bromide polymers. *Adv. Synth. Catal.* **2007**, *349*, 137−141.

(3) Menges, M. G.; Penelle, J.; Le Fevere de Ten Hove, C.; Jonas, A. M.; Schmidt-Rohr, K. Characterization of Long-Chain Aliphatic Polyesters: Crystalline and Supramolecular Structure of PE22,4 Elucidated by X-ray Scattering and Nuclear Magnetic Resonance. *Macromolecules* **2007**, *40*, 8714−8725.

(4) Alamo, R. G.; Jeon, K.; Smith, R.; Boz, E.; Wagener, K. B.; Bockstaller, M. Crystallization of polyethylenes containing chlorines: Precise vs random placement. *Macromolecules* **2008**, *41*, 7141−7151.

(5) Santonja-Blasco, L.; Zhang, X.; Alamo, R. G. Crystallization of Precision Ethylene Copolymers. In *Advances in Polymer Science*; Reiter, G.; Strobl, G. R., Eds.; Springer, 2017; pp 133−182.

(6) Zhang, X.; Santonja-Blasco, L.; Wagener, K. B.; Boz, E.; Tasaki, M.; Tashiro, K.; Alamo, R. G. Infrared spectroscopy and x-ray diffraction characterization of dimorphic crystalline structures of polyethylenes with halogens placed at equal distance along the backbone. *J. Phys. Chem. B* **2017**, *121*, 10166−10179.

(7) Zhang, X.; Zhang, W.; Wagener, K. B.; Boz, E.; Alamo, R. G. Effect of self-poisoning on crystallization kinetics of dimorphic precision polyethylenes with bromine. *Macromolecules* **2018**, *51*, 1386−1397.

(8) Zhang, X.; Zuo, X.; Ortmann, P.; Mecking, S.; Alamo, R. G. Crystallization of long-spaced precision polyacetals i: Melting and recrystallization of rapidly formed crystallites. *Macromolecules* **2019**, *52*, 4934−4948.

(9) Marxsen, S. F.; Alamo, R. G. Melt-memory of polyethylenes with halogen substitution: Random vs. precise placement. *Polymer* **2019**, *168*, 168−177.

(10) Baur, M.; Lin, F.; Morgen, T. O.; Odenwald, L.; Mecking, S. Polyethylene materials with in-chain ketones from nonalternating catalytic copolymerization. *Science* **2021**, *374*, 604−607.

(11) Häußler, M.; Eck, M.; Rothauer, D.; Mecking, S. Closed-loop recycling of polyethylene-like materials. *Nature* **2021**, *590*, 423−427.

(12) Schwab, S. T.; Baur, M.; Nelson, T. F.; Mecking, S. Synthesis and Deconstruction of Polyethylene-type Materials. *Chem. Rev.* **2024**, *124*, 2327−2351.

(13) Boz, E.; Nemeth, A. J.; Wagener, K. B.; Jeon, K.; Smith, R.; Nazirov, F.; Bockstaller, M. R.; Alamo, R. G. Well-defined precision ethylene/vinyl fluoride polymers: Synthesis and crystalline properties. *Macromolecules* **2008**, *41*, 1647−1653.

(14) Tasaki, M.; Yamamoto, H.; Hanesaka, M.; Tashiro, K.; Boz, E.; Wagener, K. B.; Ruiz-Orta, C.; Alamo, R. G. Polymorphism and phase transitions of precisely halogen-substituted polyethylene.(1) crystal structures of various crystalline modifications of bromine-substituted polyethylene on every 21st backbone carbon. *Macromolecules* **2014**, *47*, 4738−4749.

(15) Kaner, P.; Ruiz-Orta, C.; Boz, E.; Wagener, K. B.; Tasaki, M.; Tashiro, K.; Alamo, R. G. Kinetic control of chlorine packing in crystals of a precisely substituted polyethylene. toward advanced polyolefin materials. *Macromolecules* **2014**, *47*, 236−245.

(16) Schulz, M.; Seidlitz, A.; Kurz, R.; Bärenwald, R.; Petzold, A.; Saalwächter, K.; Thurn-Albrecht, T. The underestimated effect of intracrystalline chain dynamics on the morphology and stability of semicrystalline polymers. *Macromolecules* **2018**, *51*, 8377−8385.

(17) Schulz, M.; Schäfer, M.; Saalwächter, K.; Thurn-Albrecht, T. Competition between crystal growth and intracrystalline chain diffusion determines the lamellar thickness in semicrystalline polymers. *Nat. Commun.* **2022**, *13*, No. 119.

(18) Pines, A.; Rhim, W.-K.; Waugh, J. Homogeneous and inhomogeneous nuclear spin echoes in solids. *J. Magn. Reson.* **1972**, *6*, 457−465.

(19) Schäler, K.; Roos, M.; Micke, P.; Golitsyn, Y.; Seidlitz, A.; Thurn-Albrecht, T.; Schneider, H.; Hempel, G.; Saalwächter, K. Basic principles of static proton low-resolution spin diffusion nmr in nanophase-separated materials with mobility contrast. *Solid State Nucl. Magn. Reson.* **2015**, *72*, 50−63.

(20) Torchia, D. A. The measurement of proton-enhanced carbon-13 t1 values by a method which suppresses artifacts. *J. Magn. Reson.* **1978**, *30*, 613−616.

(21) Munowitz, M. G.; Griffin, R.; Bodenhausen, G.; Huang, T. Two-dimensional rotational spin-echo nuclear magnetic resonance in solids: correlation of chemical shift and dipolar interactions. *J. Am. Chem. Soc.* **1981**, *103*, 2529−2533.

(22) Wei, Y.; Graf, R.; Sworen, J. C.; Cheng, C.-Y.; Bowers, C. R.; Wagener, K. B.; Spiess, H. W. Local and collective motions in precise polyolefins with alkyl branches: A combination of 2h and 13c solid-state nmr spectroscopy. *Angew. Chem.* **2009**, *121*, 4687−4690.

(23) Schmidt-Rohr, K.; Spiess, H. Chain diffusion between crystalline and amorphous regions in polyethylene detected by 2d exchange carbon-13 nmr. *Macromolecules* **1991**, *24*, 5288−5293.

(24) Anuar, A.; Yu, Q.; Jariyavidyanont, K.; Petzold, A.; Androsch, R.; Thurn-Albrecht, T.; Saalwächter, K. Poly-3-hydroxybutyrate, a crystal-mobile biodegradable polyester. *Macromolecules* **2024**, *57*, 8507−8518.

(25) Reichert, D.; Saalwächter, K. Dipolar Coupling: Molecular-level Mobility. In *Encyclopedia of Magnetic Resonance*; Grant, D. M.; Harris, R. K., Eds.; John Wiley & Sons, Ltd, 2009; pp 177−193.

(26) Harris, R. K.; Wasylishen, R. E.; Duer, M. J. *NMR Crystallography*; John Wiley & Sons, 2009; Vol. *4*.

(27) Schäler, K.; Achilles, A.; Bärenwald, R.; Hackel, C.; Saalwächter, K. Dynamics in crystallites of poly (ε-caprolactone) as investigated by solid-state nmr. *Macromolecules* **2013**, *46*, 7818−7825.

(28) Kurz, R.; Cobo, M. F.; de Azevedo, E. R.; Sommer, M.; Wicklein, A.; Thelakkat, M.; Hempel, G.; Saalwächter, K. Avoiding bias effects in nmr experiments for heteronuclear dipole-dipole coupling determinations: Principles and application to organic semiconductor materials. *ChemPhysChem* **2013**, *14*, 3146−3155.

(29) Hackel, C.; Zinkevich, T.; Belton, P.; Achilles, A.; Reichert, D.; Krushelnitsky, A. The trehalose coating effect on the internal protein dynamics. *Phys. Chem. Chem. Phys.* **2012**, *14*, 2727−2734.

(30) Abragam, A. *The Principles of Nuclear Magnetism*; Oxford University Press, 1961.

(31) Lipari, G.; Szabo, A. Model-free approach to the interpretation of nuclear magnetic resonance relaxation in macromolecules. 1. theory and range of validity. *J. Am. Chem. Soc.* **1982**, *104*, 4546−4559.

(32) Goldman, M.; Shen, L. Spin-spin relaxation in laf$_3$. *Phys. Rev.* **1966**, *144*, No. 321.

(33) Basiura, M.; Gearba, R.; Ivanov, D.; Janicki, J.; Reynaers, H.; Groeninckx, G.; Bras, W.; Goderis, B. Rapidly cooled polyethylenes: on the thermal stability of the semicrystalline morphology. *Macromolecules* **2006**, *39*, 8399−8411.

(34) Bärenwald, R.; Champouret, Y.; Saalwächter, K.; Schäler, K. Determination of chain flip rates in poly (ethylene) crystallites by

solid-state low-field 1h nmr for two different sample morphologies. *J. Phys. Chem. B* **2012**, *116*, 13089−13097.
(35) Yu, Q.; Anuar, A.; Petzold, A.; Balko, J.; Saalwächter, K.; Thurn-Albrecht, T. The semicrystalline morphology of polybutylene succinate supports a general scheme based on intracrystalline dynamics. *Macromol. Chem. Phys.* **2023**, *224*, No. 2200459.
(36) Hu, W.-G.; Schmidt-Rohr, K. Polymer ultradrawability: the crucial role of α-relaxation chain mobility in the crystallites. *Acta Polym.* **1999**, *50*, 271−285.
(37) Tonelli, A. E. *NMR Spectroscopy and Polymer Microstructure: The Conformational Connection*; VCH: Weinheim, 1989.
(38) Bärenwald, R.; Goerlitz, S.; Godehardt, R.; Osichow, A.; Tong, Q.; Krumova, M.; Mecking, S.; Saalwächter, K. Local flips and chain motion in polyethylene crystallites: a comparison of melt-crystallized samples, reactor powders, and nanocrystals. *Macromolecules* **2014**, *47*, 5163−5173.
(39) Axelson, D. E.; Mandelkern, L.; Popli, R.; Mathieu, Pd. Carbon-13 nmr of polyethylenes: Correlation of the crystalline component t1 with structure. *J. Polym. Sci., Polym. Phys. Ed.* **1983**, *21*, 2319−2335.
(40) Yao, Y.-F.; Graf, R.; Spiess, H. W.; Lippits, D.; Rastogi, S. Morphological differences in semicrystalline polymers: Implications for local dynamics and chain diffusion. *Phys. Rev. E* **2007**, *76*, No. 060801.
(41) Yao, Y.; Graf, R.; Spiess, H.; Rastogi, S. Influence of crystal thickness and topological constraints on chain diffusion in linear polyethylene. *Macromol. Rapid Commun.* **2009**, *30*, 1123−1127.

https://doi.org/10.1021/acs.macromol.5c00349
Macromolecules 2025, 58, 3849−3859